ACS OMEGA

Open Access

http://pubs.acs.org/journal/acsodf

Article

Reduction–Sulfurization Smelting Process of Waste Hydrogenation Catalysts, Automotive Exhaust Purifier Waste Catalysts, and Laterite Nickel Ore

Zihao Wang, Haibei Wang, XiaoWu Jie, Xu Zhao, Kristian E. Waters, Derek O. Northwood, Senlin Cui, and Hao Ma*

Cite This: *ACS Omega* 2023, 8, 40713–40728

Read Online

ACCESS | Metrics & More | Article Recommendations

ABSTRACT: Reduction–sulfurization smelting is an effective method for treating solid hazardous waste and recovering valuable components from them. In this work, a waste hydrogenation catalyst (WHC), an automotive exhaust purifier waste catalyst (AEPWC), a vulcanizer, and laterite nickel ore were mixed, and the reduction smelting behavior of this solid waste was investigated. XRD (X-ray diffractometry), TG-DSC (thermogravimetric/differential scanning calorimetry), SEM-EDS (scanning electron microscopy-energy dispersive spectroscopy), OM (optical microscopy), and ICP-OES (inductively coupled plasma-optical emission spectrometry) methods were used to examine the chemical composition, thermal stability, structure, and morphology, as well as the metal content of the samples. Under the Al_2O_3-FeO-SiO_2 ternary slag system, at a smelting temperature of 1450 °C, smelting time of 2 h, mass ratio of coke, pyrite, and CaO to waste catalysts of 16, 25, and 0%, respectively, nickel (Ni) and molybdenum (Mo) recovery reached 91.1 and 92.9%, respectively, where average PGMs (platinum group metals, platinum (Pt), palladium (Pd), rhodium (Rh)) recovery reached 96%, although vanadium (V) recovery was only 25.1%. The characterization of the slag shows that Al, Si, and Fe are mainly bound in the form of chemical compounds, while V is intercalated with ferro- or aluminosilicate, which hinders the reduction and sulfurization of V. A series of tests using reduction smelting without sulfurization were also conducted, after which the Ni, Mo, and V recovery reached 96.8, 96.6, and 89.7%, respectively, while PGMs (Pt, Pd, Rh) recovery ranges from 90.2 to 98.0%. The collaborative disposal of primary ore and multisource solid waste has been achieved through two process paths: reducing smelting and reducing sulfurization smelting, which provide reference for the collaborative smelting of multisource secondary resources.

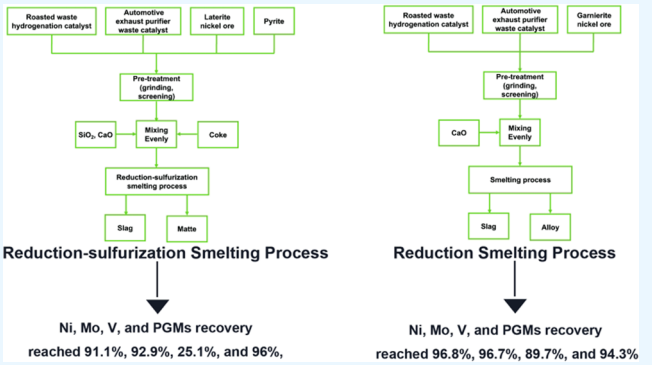

1. INTRODUCTION

80% of petroleum is processed through hydrogenation to improve its combustion quality.[1] The hydrogenation catalyst plays a vital role in this process, and the WHC usually contains a high value content of metals such as nickel, molybdenum, vanadium, and cobalt, totaling about 10–30%.[2] Platinum group metals (PGMs), in contrast, are widely used as active components of catalytic converters for the automotive exhaust purifiers. The catalytic converter was usually made from cordierite coated with γ-Al_2O_3, with over 80% of the catalytic components being platinum, palladium, and rhodium.[3−5] The function of the γ-Al_2O_3 carrier is to carry the active components, increase the specific surface area of the catalyst, and improve the reaction efficiency. The active components are the core of the hydrogenation catalyst and the main elements that can catalyze the hydrogenation reaction. Commonly used elements include nickel (Ni), copper (Cu), molybdenum (Mo), and cobalt (Co). It should be noted that the high value and catalytic activity of these metal elements make WHCs and catalytic converters highly valuable for recycling. With the explosive growth of new energy industry, the demand for key metals is increasing rapidly. Various types of spent catalysts contain a variety of valuable metals, such as molybdenum, nickel, vanadium, aluminum, rare precious metals, etc., and have become an excellent secondary resource.

Laterite nickel ores are currently the major source of nickel. Laterite nickel ores can be divided into two types: saprolitic laterite and limonitic laterite.[6] The pyrometallurgical process

Received: August 6, 2023
Accepted: October 6, 2023
Published: October 20, 2023

has become the mainstream smelting process for treating these laterite nickel ores. In general, two methods are used: reduction smelting of ferronickel and reduction−sulfurization of nickel matte.[7,8] The reduction smelting of ferronickel is the most mature technology currently used in the industry.[9] This typically uses a rotary kiln drying the prereduction electric furnace smelting process (RKEF);[10] however, the first technology to realize industrial production of laterite was reduction−sulfurization of nickel matte, where the laterite nickel ore is crushed and screened to give a fine particle size distribution. Then, a drying treatment is applied, after which the laterite nickel ore is smelted with sulfiding and reducing agents in a blast furnace or electric furnace at a temperature above 1500 °C to obtain low-grade nickel matte. This is then converted into high-grade nickel matte using a converter.[11,12] The amount of vulcanizer and reducing agent determines the grade of the low-grade nickel matte. Sulfur, pyrite, and gypsum are commonly used as sulfiding agents.[13] With the continuous increase in demand for ternary lithium battery materials (Ni, Co, Mn oxides), the reduction−sulfurization smelting process is attracting increasing attention.[14−16]

Usually, after pretreatment of spent catalysts, there are three main methods to recover valuable metals as efficiently and cleanly as possible: (1) hydrometallurgy, (2) pyrometallurgy, and (3) pyro-hydrometallurgy. Razavian et al. obtained a high-purity nickel hydroxide (>98%) from waste NiO/Al_2O_3 catalyst by sulfuric acid leaching and explored the optimal technological conditions for extracting nickel and aluminum with a sulfuric acid leaching agent.[17] For molybdenum and vanadium in spent catalysts, they can be leached as metal oxides using alkaline solutions, but the recovery of nickel and iron is difficult.[18] Laungsakulthai et al. carried out the experiment of smelting and reducing iron filings, petroleum coke, and spent nickel catalyst to produce nickel alloy and ferronickel through a laboratory induction furnace.[19] By adjusting the content of SiO_2/CaO in raw materials and smelting at 1500−1550 °C, the recovery rate of Ni reached over 98%, and FeNi40 was produced. It can be seen that it is feasible to smelt nickel from spent nickel catalyst in an induction furnace to produce nickel alloy. Pak et al. recovered nickel, molybdenum, and vanadium from waste petroleum catalysts in the form of Fe-V and Fe-Ni-Mo alloys by reduction melting at 1800 °C.[20] Ilhan et al. used a blank roasting of spent HDS catalyst at 500 °C for 4 h.[21] This not only removed the sulfur-containing carbon and other organic matter from the spent catalyst but also converted metal sulfides into metal oxides, which were then leached by oxalic acid, and the maximum leaching rate of molybdenum was 92%. Zhang et al. recovered valuable metals from the spent catalyst by adjusting the leaching pH in each section after the catalyst was roasted at 400 °C, and he recovered nickel, molybdenum, and vanadium from the spent catalyst by three stages in different alkaline solutions under optimal conditions, with recovery reaching 88.74, 97.92, and 97.13%, respectively.[22]

Collaborative use of industrial kilns is currently a mainstream technology for the comprehensive utilization of solid waste. Based on existing high-temperature industrial kilns, such as cement kilns, high-temperature boilers, and iron-making blast furnaces, solid waste can be codisposed with other materials.[23] Melendi et al. added several waste plastics and lubricating oils to the iron-making process, with the results showing that this did not reduce the quality of iron; instead, it helped reduce fuel consumption.[24] Guo et al. used two solid wastes, scrap iron oxide desulfurizer and copper smelting slag, as raw materials. Copper was effectively enriched in the dust using the reduction−sulfurization process, and copper enrichment reached 90.8%.[25] Li et al. used sulfur-containing waste gypsum as a sulfurizing agent to synergistically smelt with copper slag in a reducing atmosphere, thus enabling over 90% of Cu and Co in the copper slag to be selectively recovered.[12]

Research on the recycling of these waste catalysts mentioned above often focuses on only one type of waste catalyst. However, there are many types of waste catalysts in the industry with complex composition and uneven distribution. Despite the problems of high energy consumption and high cost, pyrometallurgy has strong adaptability to raw materials, the technology is mature, and the coordinated disposal of various spent catalysts can be achieved. In the meanwhile, based on the trapping effect of copper, nickel, iron, and other elements on rare and precious metals, a comprehensive recovery of valuable metals in multisource spent catalysts can be realized.

Smelting WHC and AEPWC together with laterite nickel ore can help recover valuable components and effectively reduce the ecological damage caused by the disposal of these two types of hazardous waste.[26] The main process of collaborative reduction−sulfurization of multisource solid wastes in this project uses pyrite as the vulcanizing agent and coke as the reducing agent. Valuable metal oxides such as nickel, molybdenum, vanadium, and some iron oxides are reduced to their elemental state. The reduced elemental iron can also reduce valuable metal oxides while also undergoing an interactive vulcanizing reaction with pyrite, forming a low-grade nickel matte that is composed of metal sulfides such as iron sulfide and nickel sulfide. The matte can be easily separated from the slag. Additionally, the matte also serves as a trapping agent for precious metals including PGMs.

2. MATERIALS AND METHODS

2.1. Materials and Analysis. The WHC and AEPWC were provided by two individual Chinese environmental companies located in Langfang, Hebei Province, and Xuzhou, Jiangsu Province, respectively. The laterite nickel ore, together with the vulcanizing and reducing agents of pyrite and coke, was provided by a nickel−cobalt mine on Sulawesi Island (Indonesia). Other additives including CaO and SiO_2 were analytically pure and purchased from Sinopharm Chemical Reagent Co., Ltd. The phase composition of the samples was investigated by X-ray diffractometry (XRD, D8 Advance, Bruker, Germany). Metal content analysis was performed using an inductively coupled plasma-optical emission spectrometer (ICP-OES, 730, Agilent). Thermogravimetric analysis of the waste catalysts was performed by using a thermogravimetric/differential scanning calorimeter (TG-DSC, STA 449 F5, Netzsch, Germany). It should be noted that in order to better simulate the smelting atmosphere of the reduction test, the thermogravimetric analysis uses an air atmosphere with a heating rate of 10°/min. The chemical states of metal elements were analyzed by X-ray energy dispersive spectroscopy (EDS, Genesis 7000, EDAX). The morphologies of the samples were examined using scanning electron microscopy (SEM, Axioplan 2, Zeiss, Germany).

2.2. Reduction−Sulfurization Smelting Process. Three steps were involved with the reduction−sulfurization smelting process: these steps are (1) Pretreatment: AEPWC, WHC, laterite nickel ore, and pyrite were finely ground to pass 100

https://doi.org/10.1021/acsomega.3c05772
ACS Omega 2023, 8, 40713−40728

mesh by a vibrating mill; (2) Mixing: Based on the lower melting point zone of the Al_2O_3-FeO-SiO_2 ternary slag system, 40 g of roasted WHC, 40 g of AEPWC, 120 g of laterite nickel ore, 64 g of SiO_2 as well as a set mass of coke, pyrite, and CaO were mixed in a sealed bag and shook for 5 min to reach uniform mixing; (3) Smelting: The mixed raw materials were loaded into a corundum crucible, and then, the crucible was put in the furnace at a set temperature for a predetermined time according to the experimental plan. Pyrite, as a sulfurizer, forms a matte body under high-temperature conditions. The reduced valuable metal enters the matte phase due to its sulfur affinity and the "washing" and precipitation of the matte body.[27] Due to the difference in density, the matte phase settles at the bottom of the crucible and thus is separated from the slag phase. At the end of the test, the crucible was naturally cooled to room temperature and then the matte and slag were sent for metal analysis. The flowsheet of the complete reduction−sulfurization smelting process is shown in Figure 1.

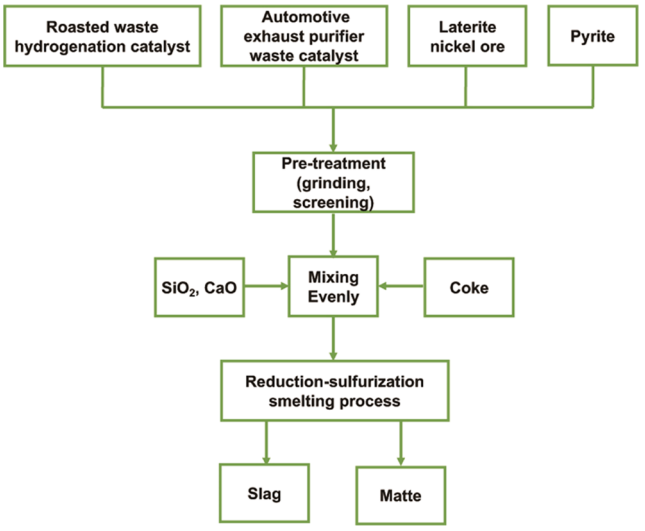

Figure 1. Process flowsheet for the reduction−sulfurization smelting process.

Metal recovery was calculated using eq 1[28,29]

$$r = \left(1 - \frac{M_2 * Z_X}{M_1 * C_X}\right) * 100\% \quad (1)$$

where r is the metal recovery in %, M_1 and M_2 represent the weight of the raw materials and slag in grams (g), C_x and Z_x refer to the metal content of raw materials and slag in weight percent (wt %). the mass of the metal element in the solution in grams (g), and W_R is the mass of the metal element in the residue in grams (g). X presents Ni, Mo, V, Pt, Pd, and Rh.

3. RESULTS AND DISCUSSION

3.1. Materials Characterization. *3.1.1. WHC.* The chemical composition of WHC is shown in Table 1.

After fine grinding, the weight loss of the WHC after heating was analyzed by thermogravimetric analysis over the temperature range of 25−1000 °C. The TG curve is shown in Figure 2a.

It can be seen from Figure 2a that as the temperature increases, the catalyst undergoes significant weight loss, which can be divided into two stages: the first stage is at 25−320 °C, with a weight loss of 11.8 wt %. It is inferred that the oily substances on the surface of the WHC are decomposed and volatilized by heat. The second stage is from 320 to 840 °C with a weight loss rate of 32.8%. The weight loss rate (%/°C) is the fastest within the range of 320−430 °C. After 840 °C, the TG curve tends to flatten, and the weight of the spent hydrogenation catalyst remains unchanged.

To have a better control of slag volume and avoidance of excessive feeding, the catalyst was roasted at 750 °C for 2 h before any smelting test. The weight loss rate is 46.8%/°C, which is in agreement with the thermogravimetric analysis. The main chemical composition of the catalyst after roasting (wt %) is shown in Table 2.

The XRD patterns of the raw and roasted catalyst are shown in Figure 3a,b. After roasting, the materials in the WHC are all oxides, with the main constituent being Al_2O_3. A small amount of Fe exists in the form of Fe_3O_4. Ni and Mo were oxidized and formed nickel molybdate ($NiMoO_4$), and V was oxidized to V_2O_5.

3.1.2. AEPWC. The chemical composition of AEPWC is given in Table 3.

A thermogravimetric analysis over the temperature range of 25−1000 °C was also performed on the catalyst, and the results are shown in Figure 2b.

Figure 2b shows that the spent automotive catalyst is relatively stable at high temperatures, and as the temperature increases, the mass change is insignificant, resulting in only a net 1.27% weight loss. The thermogravimetric curve can be divided into two stages: within the range of 25−540 °C, the weight loss rate of the sample is 1.63%, and as the temperature gradually increases, the weight loss rate tends to slow down. The initial faster loss rate may be due to the volatilization of carbon and other substances contained in the sample; within the range of 540−1000 °C, the mass of the sample slowly increases with the increase of temperature, indicating that some substances have undergone oxidation reactions that have increased their weight. Based on these data, the catalyst was used as is.

The XRD pattern of the catalyst is shown in Figure 3c. The main diffraction peaks are from cordierite ($Mg_2Al_4Si_5O_{18}$). Other compounds do not show obvious diffraction peaks due to either low content or being amorphous. Cordierite is quite stable and is not easily changed by heating. γ- Al_2O_3 coats the entire surface and at high temperatures, γ-Al_2O_3 transforms into α-Al_2O_3, and PGMs are stably encapsulated on the catalyst surface in the form of fine particles.

3.1.3. Laterite Nickel Ore. The chemical composition of laterite nickel ore is given in Table 4.

It can be seen from Table 4 that this type of nickel ore has a typical characteristic of high Fe, low Ni, Si, and Mg. The XRD pattern of the ore is shown in Figure 3d. The main minerals in the ore are goethite (FeO(OH)) and hematite (Fe_2O_3), which

Table 1. Chemical Composition of the WHC

element	Ni	Mo	V	Co	Fe	Al_2O_3	SiO_2	MgO	CaO	C	S
content (wt %)	3.44	3.99	3.16	0.05	1.04	33.65	1.09	0.13	0.42	23.76	7.12

https://doi.org/10.1021/acsomega.3c05772
ACS Omega 2023, 8, 40713−40728

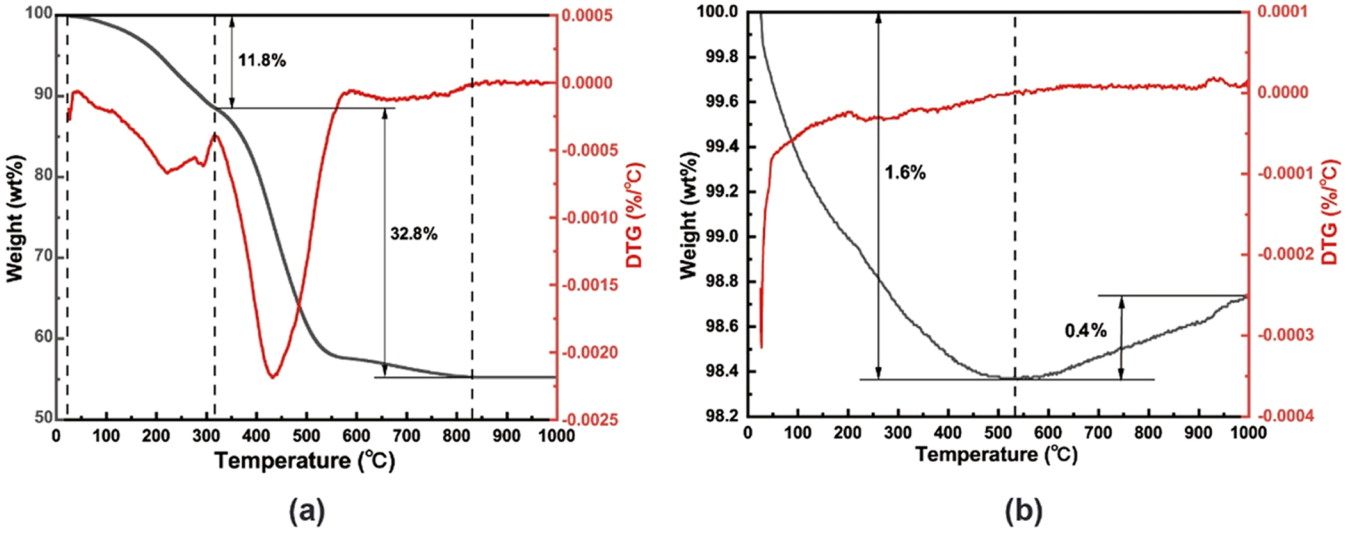

Figure 2. TG curves of (a) WHC and (b) AEPWC.

Table 2. Chemical Composition of the WHC after Roasting

element	Ni	Mo	V	Co	Fe	Al_2O_3	SiO_2	CaO	C	S
content (wt %)	6.41	7.15	5.26	0.18	1.76	61.75	1.52	0.63	0.03	0.32

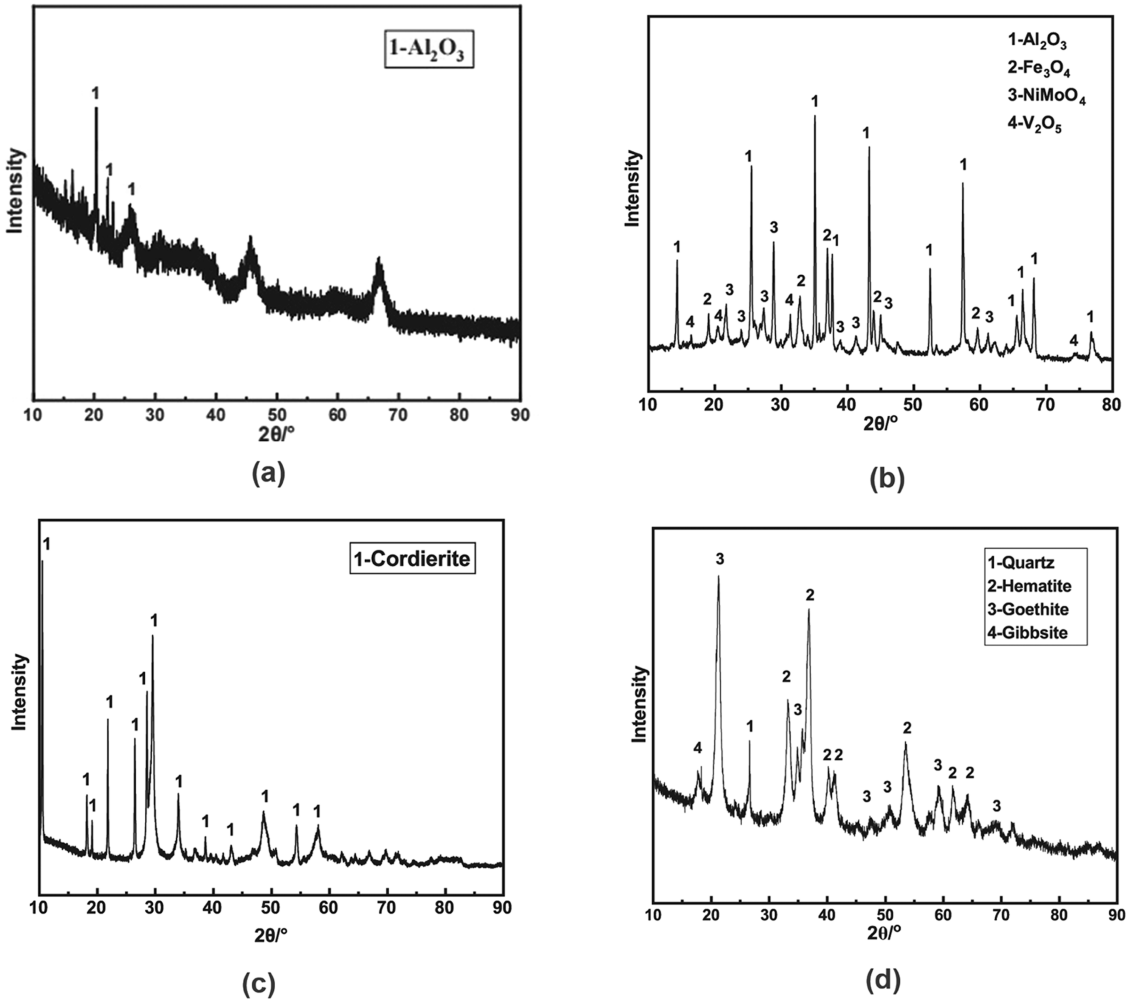

Figure 3. XRD patterns of (a) raw WHC, (b) WHC after roasting, (c) spent automotive catalyst, and (d) limonitic laterite ore.

https://doi.org/10.1021/acsomega.3c05772
ACS Omega 2023, 8, 40713−40728

Table 3. Chemical Composition of the AEPWC

element	Al_2O_3	SiO_2	Fe_2O_3	CaO	MgO	Ce	Zr	La	Pt	Pd	Rh
content (wt %)	38.09	37.2	0.3	0.43	10.28	2.5	3.24	0.29	13.70 g/t	131.79 g/t	10.00 g/t

Table 4. Chemical Composition of the Laterite Nickel Ore

element	Al_2O_3	SiO_2	CaO	MgO	Fe	Ni	Co	Cr
content (wt %)	6.18	3.83	0.04	0.22	52.99	1.05	0.06	1.09

Table 5. Main Compositions of Pyrite

element	Fe	Zn	Al	Ca	Mg	P	S	Si
content (wt %)	34.80	9.78	0.41	0.42	0.13	0.55	41.78	1.73

account for 95.8% of the total content. The content of gibbsite ($Al(OH)_3$) and quartz (SiO_2) is low, where only one peak for each was detected in the XRD pattern. Iron mainly occurs in goethite and hematite.

3.1.4. Pyrite and Coke. As a high-quality reducing agent, coke used in this project had a high fixed carbon content of 83.49 wt %, with ash and volatile contents of 15.54 and 1.97 wt %, respectively. The main compositions of pyrite are given in Table 5. Pyrite is mainly composed of Fe and S, with contents of 34.80 and 41.78%, respectively. It also contains 9.78% Zn.

3.2. Thermodynamic Analysis. Thermodynamic analysis can be used to study the possibility and limit of reactions in the smelting process as well as to study the influence of parameters such as temperature and pressure on the reaction, thereby exploring whether pyrometallurgical reactions can happen under given conditions. HSC Chemistry 9.0 and Origin software were used to draw the $\Delta G^{\theta}-T$ relationships for reactions 1−30.

Figure 4a,b gives the relationship of $\Delta G^{\theta}-T$ of FeO/Fe and FeS produced by reductive vulcanization of metal oxides and carbon, respectively.

It can be seen from Figure 4a,b that the standard Gibbs free energy of all reactions decreases with an increasing temperature. All reactions can occur below 600 °C. At approximately 200 °C, NiO and MoO_3 begin to react. However, NiO, MoO_3, and V_2O_5 require a higher temperature for the reduction−vulcanization reaction to occur. Therefore, the order in which valuable metal oxides are reduced and sulfurized by pyrite and C is MoO_3 > NiO > V_2O_5. Iron oxides can also be reduced and sulfurized by FeS_2 and C at temperatures exceeding 400 °C. To produce FeS, and compared to FeO, the higher the temperature, the easier the reduction and sulfurization of Fe_2O_3 become.

It should be noted that based on Boudouard reactions, as the temperature increases, the concentration of CO in the gas phase increases. The reaction of C and CO_2 into CO is most pronounced at 700−900 °C, and when the temperature exceeds 1000 °C, the CO concentration approaches 100%. Figure 4c,d gives the relationship of $\Delta G^{\theta}-T$ of FeO/Fe and FeS produced by reductive vulcanization of metal oxides and CO, respectively.

It can be seen from Figure 4c that NiO, MoO_3, and V_2O_5 can be reduced and sulfurized by FeS_2 and CO to produce FeO or Fe and other metal sulfides. As ΔG^{θ} for all reactions is less than zero, and the change in standard Gibbs free energy for MoO_3 and V_2O_5 shows a similar trend, and as the temperature increases, it forms a "V-shaped" pattern for ΔG^{θ} vs T. However, for NiO, ΔG^{θ} constantly decreases, and at a temperature above 600 °C, ΔG^{θ} decreases at a faster rate. The lowest ΔG^{θ} for MoO_3 and V_2O_5 occurs at 800 and 700 °C, respectively. The V_2O_5 reaction is more difficult to carry out because of its higher ΔG^{θ}. Figure 4d shows that all reactions can occur spontaneously, and ΔG^{θ} gradually decreases as the temperature increases. In the high-temperature range (above 1000 °C), the NiO reaction has the lowest ΔG^{θ}, under which conditions it is most likely to be reduced and sulfurized. Similarly, FeO is the most difficult to reduce and sulfurize.

It can be concluded that NiO, MoO_3, V_2O_5, Fe_2O_3, and FeO are more likely to undergo reductive vulcanization with C and FeS_2 at temperatures above 800 °C. Overall, the order in which various metal oxides are reduced and sulfurized by carbon and FeS_2 is NiO > MoO_3 > V_2O_5 > Fe_2O_3 > FeO. Ni, Mo, and V sulfides as well as FeS are more easily generated within the entire system, as their reaction ΔG^{θ} is lower.

Figure 4e shows the relationship of $\Delta G^{\theta}-T$ of the cross-vulcanization of valuable metal oxides with FeS_2 or FeS.

As shown above, Ni has sulfur affinity significantly stronger than that of Mo and V. As the temperature increases, the change of ΔG^{θ} for various metal oxides reacting with FeS_2 is greater when compared with the ΔG^{θ} of reactions with FeS. NiO and MoO_3 undergo an interactive vulcanization reaction with FeS_2 before V_2O_5, and the reaction begins at about 700 °C. V_2O_5 can only react with FeS_2 at temperatures above 1000 °C and cannot spontaneously undergo interactive vulcanization with FeS within the experimental temperature range (0−1500 °C). The interactive vulcanization reaction between MoO_3 and FeS also has difficulty taking place within the same temperature range.

The main slagging components contained in both catalysts are Al_2O_3 and SiO_2. Due to the lower melting point of the matte, to present the matte phase becoming embedded in the slag phase due to the high melting temperature, an Al_2O_3-FeO-SiO_2 slag with a lower melting temperature was selected for further investigation. This was supplemented by a high iron content provided by nickel laterite ore for slag formation.

3.3. Reduction−Sulfurization Smelting Process. For the smelting process investigation, 40 g of roasted WHC, 40 g of spent automotive catalyst, 120 g of laterite nickel ore, and 64 g of SiO_2 were used for each test. The effect of operating parameters, including coke addition, pyrite addition, smelting temperature, smelting time, and CaO addition, on the valuable metal recovery was investigated. The values of each parameter were chosen as follows: Coke addition ranges from 12 to 20%; pyrite addition ranges from 15 to 35%; smelting temperature ranges from 1375 to 1475 °C; smelting times range from 1.0 to 2.5 h; and CaO addition ranges from 0 to 25%. It should be noted that coke, pyrite, and CaO addition is the weight ratio of the ingredient to both catalysts (80 g).

https://doi.org/10.1021/acsomega.3c05772
ACS Omega 2023, 8, 40713−40728

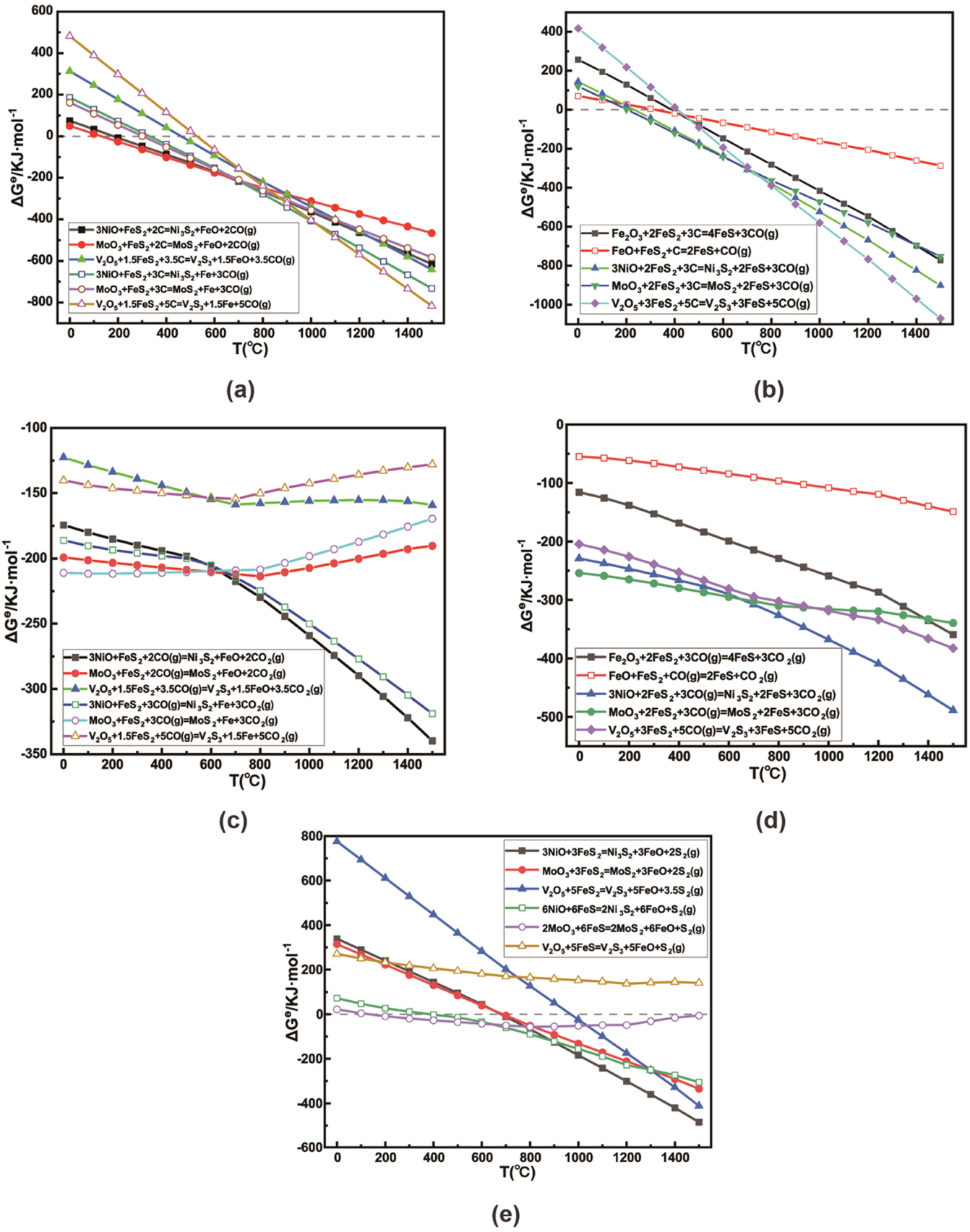

Figure 4. Relationship of $\Delta G^{\theta}-T$ for (a) FeO/Fe and (b) FeS produced by reductive vulcanization of metal oxides and C, (c) FeO/Fe and (d) FeS produced by reductive vulcanization of metal oxides and CO, and (e) vulcanization of valuable metal oxides with FeS_2 or FeS.

https://doi.org/10.1021/acsomega.3c05772
ACS Omega 2023, 8, 40713−40728

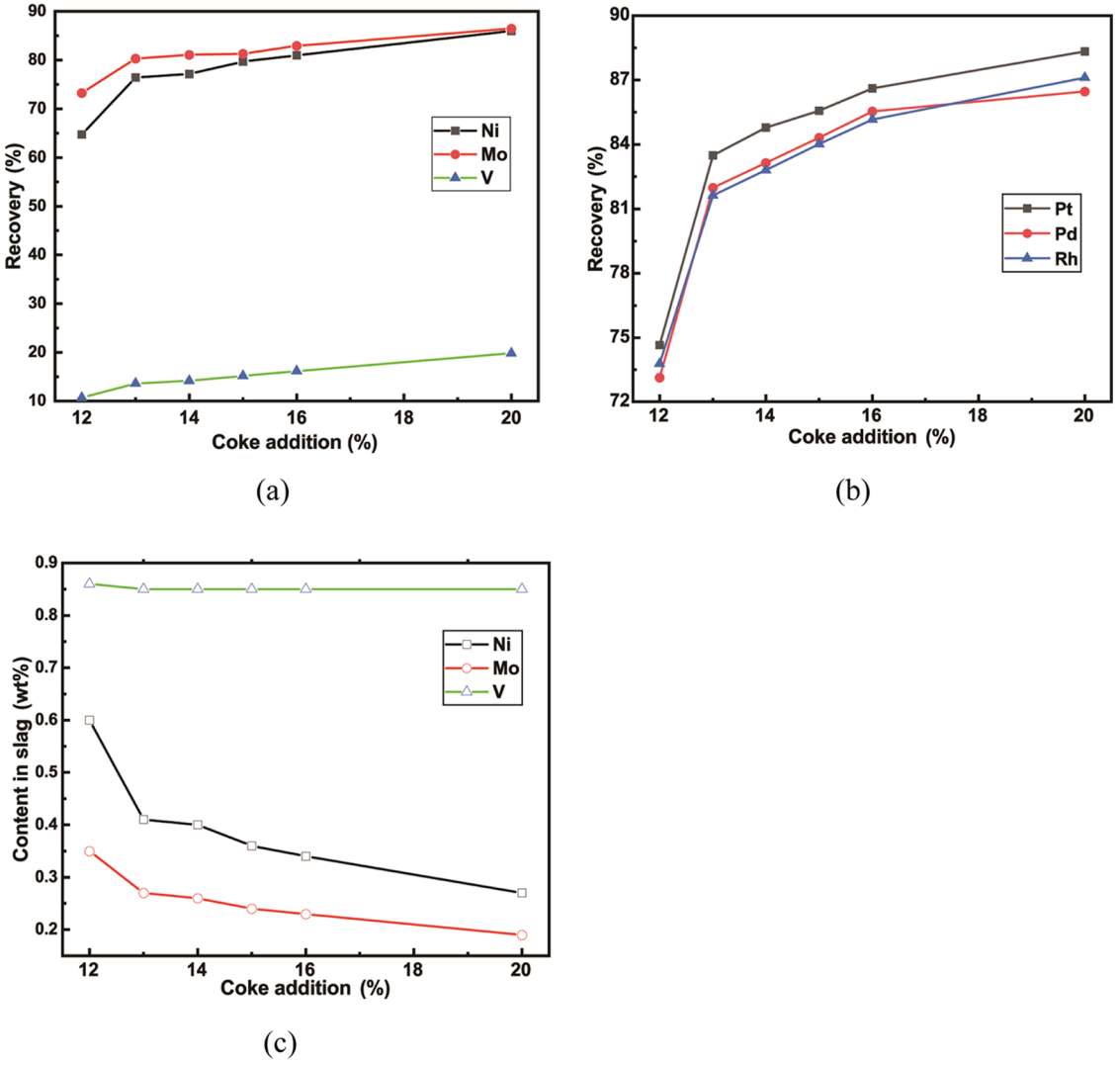

Figure 5. Effect of coke addition on (a) Ni/Mo/V recovery, (b) PGMs recovery, and (c) content of Ni/Mo/V in the slag.

The main chemical reactions that can occur during the reduction−sulfurization smelting process include[30,31]

$$3NiO + FeS_2 + 2C = Ni_3S_2 + FeO + 2CO(g) \quad (2)$$

$$MoO_3 + FeS_2 + 2C = MoS_2 + FeO + 2CO(g) \quad (3)$$

$$V_2O_5 + 1.5FeS_2 + 3.5C = V_2S_3 + 1.5FeO + 3.5CO(g) \quad (4)$$

$$3NiO + FeS_2 + 3C = Ni_3S_2 + Fe + 3CO(g) \quad (5)$$

$$MoO_3 + FeS_2 + 3C = MoS_2 + Fe + 3CO(g) \quad (6)$$

$$V_2O_5 + 1.5FeS_2 + 5C = V_2S_3 + 1.5Fe + 5CO(g) \quad (7)$$

$$Fe_2O_3 + 2FeS_2 + 3C = 4FeS + 3CO(g) \quad (8)$$

$$FeO + FeS_2 + C = 2FeS + CO(g) \quad (9)$$

$$3NiO + 2FeS_2 + 3C = Ni_3S_2 + 2FeS + 3CO(g) \quad (10)$$

$$MoO_3 + 2FeS_2 + 3C = MoS_2 + 2FeS + 3CO(g) \quad (11)$$

$$V_2O_5 + 3FeS_2 + 5C = V_2S_3 + 3FeS + 5CO(g) \quad (12)$$

The C−O system inevitably undergoes continuous reactions with temperature changes. With the gradual increase of temperature and under the control of the Boudouard reaction, the reduction atmosphere in the furnace is gradually dominated by CO, and the main reactions that can occur between metal oxide and pyrite and CO include[32−34]

$$3NiO + FeS_2 + 2CO(g) = Ni_3S_2 + FeO + 2CO_2(g) \quad (13)$$

$$MoO_3 + FeS_2 + 2CO(g) = MoS_2 + FeO + 2CO_2(g) \quad (14)$$

$$V_2O_5 + 1.5FeS_2 + 3.5CO(g) = V_2S_3 + 1.5FeO + 3.5CO_2(g) \quad (15)$$

$$3NiO + FeS_2 + 3CO(g) = Ni_3S_2 + Fe + 3CO_2(g) \quad (16)$$

$$MoO_3 + FeS_2 + 3CO(g) = MoS_2 + Fe + 3CO_2(g) \quad (17)$$

$$V_2O_5 + 1.5FeS_2 + 5CO(g) = V_2S_3 + 1.5Fe + 5CO_2(g) \quad (18)$$

https://doi.org/10.1021/acsomega.3c05772
ACS Omega 2023, 8, 40713−40728

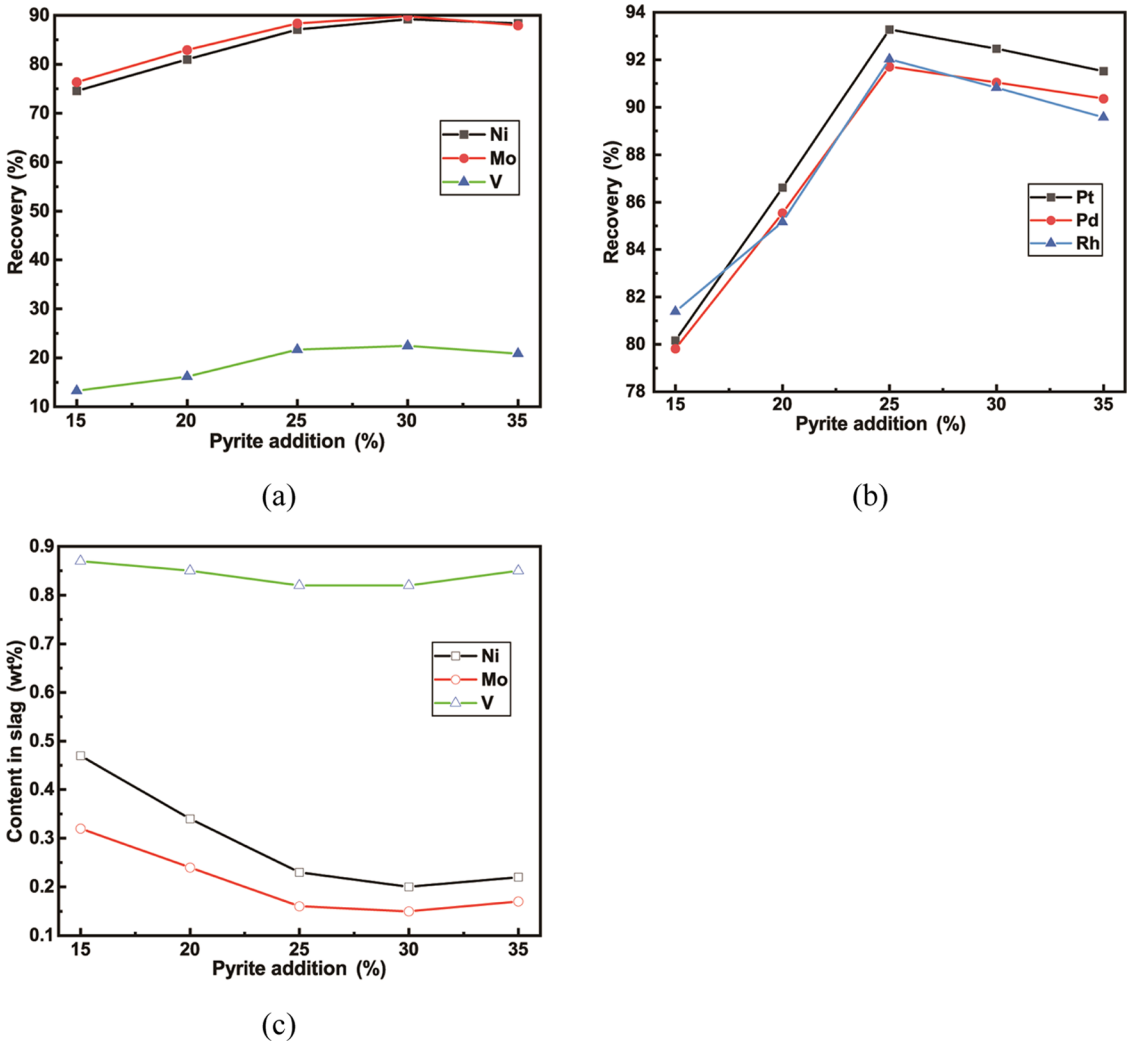

Figure 6. Effect of pyrite addition on (a) Ni/Mo/V recovery, (b) PGMs recovery, and (c) content of Ni/Mo/V in the slag.

$$Fe_2O_3 + 2FeS_2 + 3CO(g) = 4FeS + 3CO_2(g) \quad (19)$$

$$FeO + FeS_2 + CO(g) = 2FeS + CO_2(g) \quad (20)$$

$$3NiO + 2FeS_2 + 3CO(g) = Ni_3S_2 + 2FeS + 3CO_2(g) \quad (21)$$

$$MoO_3 + 2FeS_2 + 3CO(g) = MoS_2 + 2FeS + 3CO_2(g) \quad (22)$$

$$V_2O_5 + 3FeS_2 + 5CO(g) = V_2S_3 + 3FeS + 5CO_2(g) \quad (23)$$

When oxygen is not sufficient, high-valent sulfides are prone to decomposition reactions[35]

$$FeS_2 = FeS + 0.5S_2(g) \quad (24)$$

$$3NiS = Ni_3S_2 + 0.5S_2(g) \quad (25)$$

Low-valent sulfides are more stable at high temperatures and have lower melting points. They are sulfides that form covalent bonds between metal atoms and sulfur atoms, and they are mutually soluble to form corresponding nickel matte (Ni_3S_2-FeS) in the molten state.[36]

It should be noted that due to the oxygen affinity of Fe and the sulfur affinity of metal elements such as Ni, direct interactive sulfidation reactions that may occur between valuable metal oxides and FeS_2 or FeS include[37−383940]

$$3NiO + 3FeS_2 = Ni_3S_2 + 3FeO + 2S_2(g) \quad (26)$$

$$MoO_3 + 3FeS_2 = MoS_2 + 3FeO + 2S_2(g) \quad (27)$$

$$V_2O_5 + 5FeS_2 = V_2S_3 + 5FeO + 3.5S_2(g) \quad (28)$$

$$6NiO + 6FeS = 2Ni_3S_2 + 6FeO + S_2(g) \quad (29)$$

$$2MoO_3 + 6FeS = 2MoS_2 + 6FeO + S_2(g) \quad (30)$$

$$V_2O_5 + 5FeS = V_2S_3 + 5FeO + S_2(g) \quad (31)$$

3.3.1. Effect of Coke Addition. The coke addition ratio ranged from 12 to 20%, while the smelting temperature was 1400 °C, smelting time was 1.5 h; pyrite addition of 20%, and CaO addition of 0. It should be noted that CaO can help increase the fluidity of slag; however, the selection of 0 CaO assumes good viscosity of the Al_2O_3-FeO-SiO_2 ternary slag as well as avoiding the Al_2O_3-FeO-SiO_2-CaO quaternary slag if unnecessary. The effect of coke addition on the recovery of Ni/Mo/V and PGMs, as well as the content of Ni/Mo/V in the slag during the smelting process, was examined. The test results are listed in Figure 5.

https://doi.org/10.1021/acsomega.3c05772
ACS Omega 2023, 8, 40713−40728

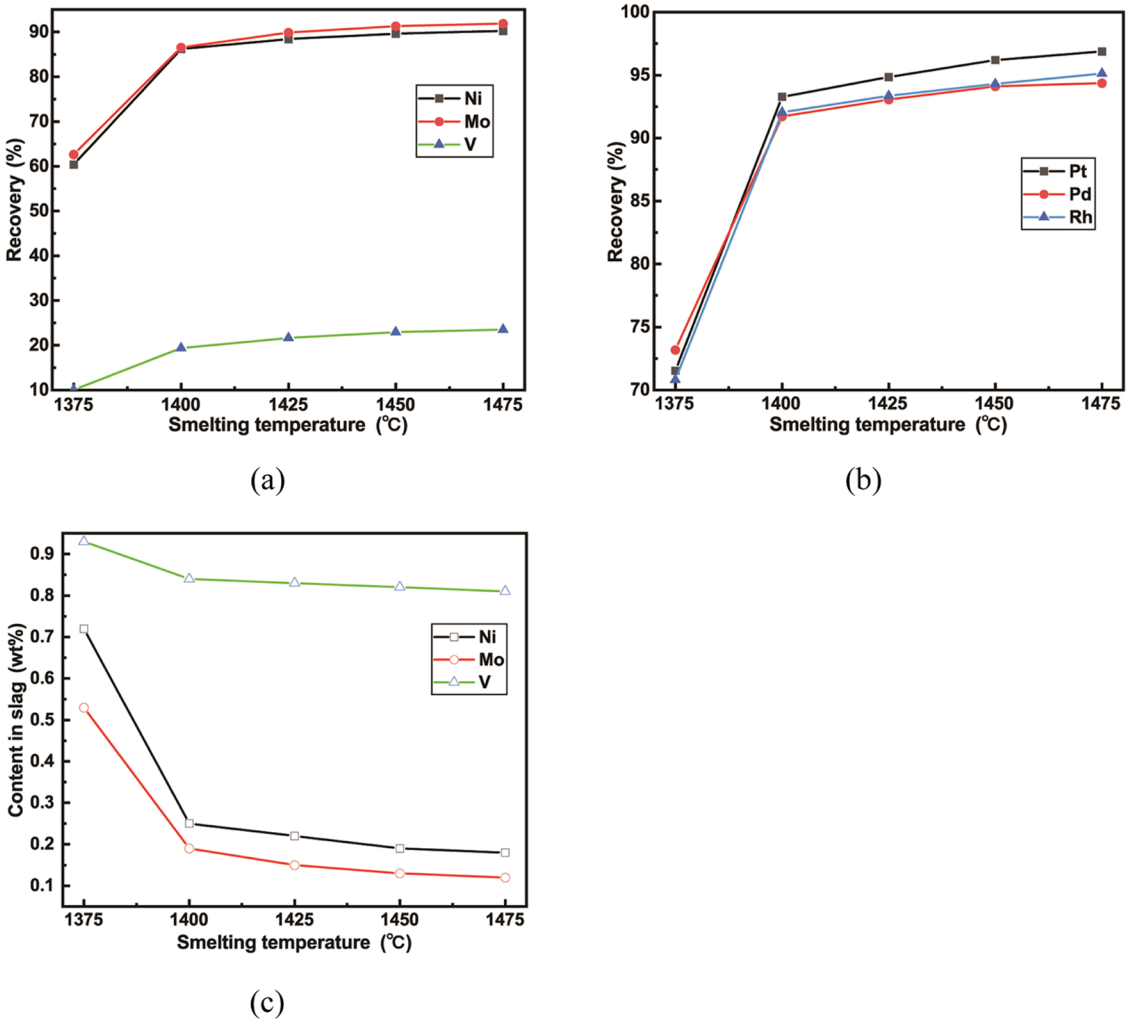

Figure 7. Effect of smelting temperature on (a) Ni/Mo/V recovery, (b) PGMs recovery, and (c) content of Ni/Mo/V in the slag.

Figure 5a shows that as the amount of coke gradually increases, the recovery of Ni, Mo, and V also gradually increases. As the number of coke increases from 12 to 20%, the recovery rates of Ni, Mo, and V increase from 64.7, 73.3, and 10.7% to 86.0, 86.5, and 19.8%, respectively. However, the recovery of V is much lower than that of Ni and Mo. This is because Ni and Mo are preferentially reduced compared to V. The sulfur affinity of V is also much lower than that of Ni and Mo.

Figure 5b shows that when the amount of coke increased from 12 to 16%, the recovery of Pt, Pd, and Rh rapidly increased from 74.7, 73.1, and 73.8% to 86.6, 85.5, and 85.2%, respectively. However, with the continued increase in the amount of coke, a large amount of Fe in the material was reduced into the mat, causing a decrease in FeO/SiO_2 in the slag, thus, also bringing an increase in slag viscosity. This resulted in a decrease in the separation between the matte and the slag phase. This, in turn, affects the enrichment of the PGMs.

Figure 5c shows that as the coke gradually increases, the Ni and Mo contents in the slag gradually decrease. The Ni and Mo contents in the slag decreased from 0.60 and 0.35 to 0.27 and 0.19%, respectively. However, the V content in the slag remains relatively unchanged, further indicating that changes in reducing agents have a poor impact on the recovery rate of V. Thus, based on the above information, coke addition was set at 16%.

3.3.2. Effect of Pyrite Addition. The test conditions were set as follows: smelting temperature of 1400 °C; smelting time of 1.5 h; coke addition of 16%; and CaO addition of 0. The pyrite addition ranged from 15% up to 35%, with an increase of 5% for each test. The effect of pyrite addition on the recovery of Ni/Mo/V, PGMs, as well as the content of Ni/Mo/V in the slag are shown in Figure 6.

It can be seen from Figure 6a that with the gradual increase in pyrite content, the recovery of Ni, Mo, and V increases in the beginning and reaches a maximum with a 30% pyrite addition, and then the recovery decreases. The maximum recovery of Ni, Mo, and V is 89.2, 89.9, and 22.4% respectively. The recycling effect of V is still not ideal compared to Ni and Mo. Figure 6b shows that as the pyrite addition increases, the recovery of Pt, Pd, and Rh first increases and then decreases. With an increase in pyrite from 15 to 25%, the Pt recovery rate increases from 80.2 to 93.3%, the Pd recovery increases from 79.8 to 91.7%, and the Rh recovery increases from 81.4 to 92.0%. It can be seen that the effect of pyrite addition on the recovery of PGMs is more significant than that of coke. However, when the pyrite content exceeds 25%, the PGMs' recovery begins to decrease slightly. Figure 6c shows that when the pyrite addition is gradually increased from 15 to 30%, the

https://doi.org/10.1021/acsomega.3c05772
ACS Omega 2023, 8, 40713−40728

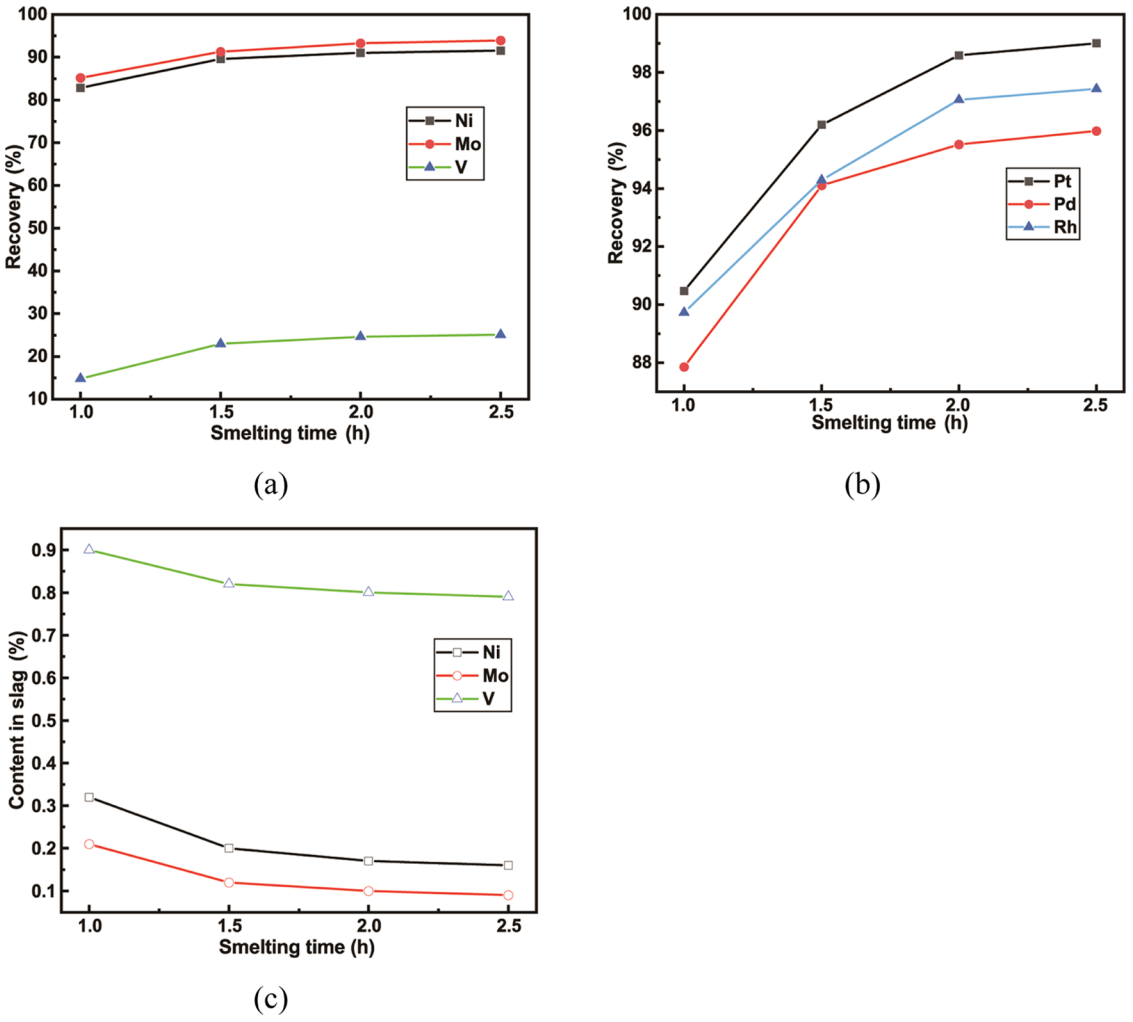

Figure 8. Effect of smelting time on (a) Ni/Mo/V recovery, (b) PGMs recovery, and (c) content of Ni/Mo/V in the slag.

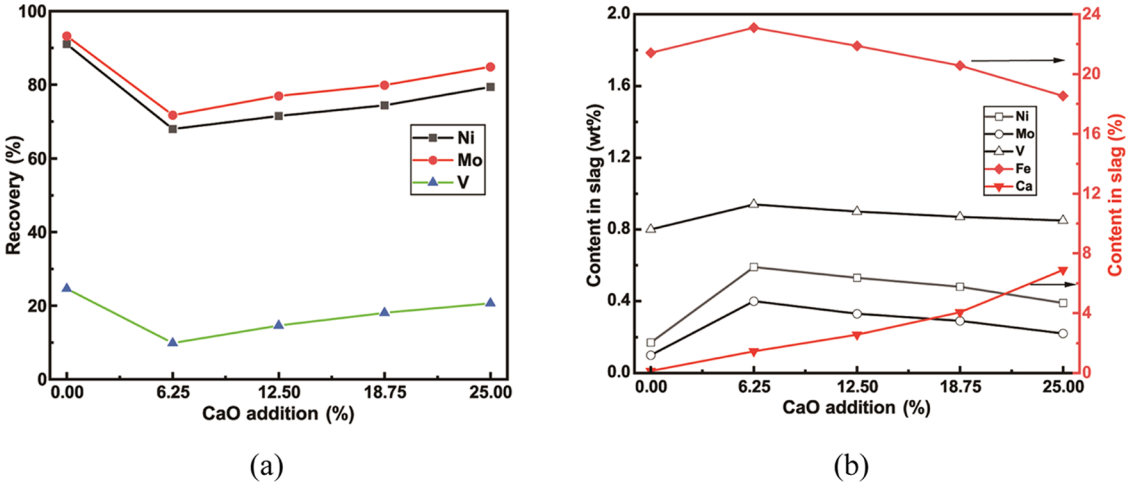

Figure 9. Effect of CaO addition on the recovery of (a) Ni/Mo/V and (b) content of main valuable metals in the slag.

contents of Ni, Mo, and V in the slag gradually decrease. When the pyrite content exceeds 30%, the content of all three metals in the slag slightly increases. This is because the FeS matte, generated from pyrite in the high-temperature smelting process, will react with Ni, Mo, V, and other valuable metals to form their sulfides. At the same time, the slag will be "washed" and "diluted" during the aggregation process to bring the valuable metals into nickel matte. Therefore, for valuable metals such as Ni, Mo, and V, pyrite behaves as a solvent. An increase in the pyrite content also increases the solubility of the valuable metal elements, and thus the content of valuable metals in the slag gradually decreases. It should be noted that

https://doi.org/10.1021/acsomega.3c05772
ACS Omega 2023, 8, 40713−40728

Table 6. Recovery of Valuable Metals for Validation Tests

no.	Ni (%)	Mo (%)	V (%)	Pt (%)	Pd (%)	Rh (%)
1	91.2	93.1	25.2	99.2	96.4	97.6
2	90.9	92.8	25.1	98.8	96.0	97.2
3	91.2	92.9	25.1	98.9	96.3	97.5
average	91.1	92.9	25.1	99.0	96.2	97.4

an excess of pyrite will lead to very high FeO content in the slag, which will reduce the interfacial tension between slag and matte, hindering the aggregation and sedimentation of valuable metal particles, thereby affecting their recovery. Thus, based on the above information, the pyrite addition was selected to be 25%.

3.3.3. Effect of Smelting Temperature. The test conditions were as follows: smelting time of 1.5 h; coke addition of 16%; pyrite addition of 25%; and CaO addition of 0. The smelting temperature ranged from 1375 to 1475 °C with 25 °C increments for each test. The results are shown in Figure 7.

As seen in Figure 7, an increase in the smelting temperature produces an increase in the recovery of Ni, Mo, and V (Figure 7a). When the smelting temperature increases from 1375 °C, which is close to the melting point temperature of the slag, to 1400 °C, the recovery of Ni, Mo, and V rapidly increases from 60.4, 62.6, and 10.1% to 86.2, 86.5, and 19.4%, respectively. Continuing to heat up to 1450 °C, the recovery of all three metals increased by more than 3%. Continuing to increase the temperature to 1475 °C, the recovery of Ni, Mo, and V showed very little change. The recovery of PGMs also increases with an increase in the temperature (Figure 7b), and the recovery is also the lowest at a smelting temperature of 1375 °C. This indicates that at this temperature, the viscosity of the slag is relatively high and is not therefore conducive to the separation of valuable metals from the slag. As the smelting temperature is gradually increased from 1400 to 1475 °C, the rate of increase in PGMs recovery also decreases and tends to flatten out after reaching 1450 °C. When the smelting temperature increases from 1375 to 1400 °C, the Ni and Mo contents in the slag drop sharply from 0.72 and 0.53% to 0.25 and 0.19%, respectively (Figure 7c). The change in V content is relatively small but it also decreases from 0.93 to 0.84%. As the temperature continues to increase, the content of Ni, Mo, and V in the slag gradually decreases, and the rate of change gradually decreases. Based on the above analysis, a smelting temperature of 1450 °C was selected.

3.3.4. Effect of Smelting Time. Smelting times of 1.0 1.5, 2.0, and 2.5 h were tested. The test conditions were as follows: smelting temperature of 1450 °C; coke addition of 16%; pyrite addition of 25%; CaO addition of 0. The results are shown in Figure 8.

As the smelting time increases, the recovery of Ni, Mo, and V gradually increases. When the smelting time was 2 h, the recovery rates of Ni, Mo, and V reached 82.9, 85.2, and 14.8%, respectively. With a further increase in smelting time from 2 to 2.5 h, the recovery of the three metals is only marginally increased. Under the same conditions, by increasing the smelting time from 1 to 2.5 h, the recovery of Pt, Pd, and Rh

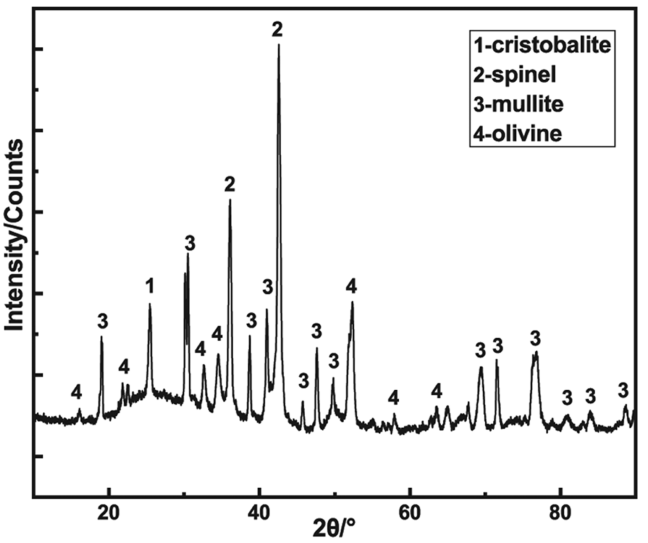

Figure 10. X-ray diffraction (XRD) analysis of the smelting slag.

increased from 90.5, 87.9, and 89.7% to 99.0, 96.0, and 97.4%, respectively. When the smelting time is 1 h, the sulfurization reduction reaction is not complete, which leads to incomplete capture of PGMs by the matte. The decrease in temperature increases the viscosity of the slag, resulting in relatively fewer PGMs entering the matte.

An increase in the smelting time also gradually reduces the content of Ni/Mo/V in the slag, with Ni, Mo, and V contents in the slag decreasing from 0.32, 0.21, and 0.90% to 0.16, 0.09, and 0.79%, respectively. Based on the above information, a smelting time of 2 h was selected.

3.3.5. Effect of CaO Addition. CaO can reduce the viscosity and density of the slag, improving its fluidity; thus, it may promote the recovery of valuable metals in the matte. The test conditions were as follows: smelting temperature 1450 of °C; smelting time of 2 h, coke addition of 16%; and pyrite addition of 25%. CaO additions of 0, 6.25, 12.5, 18.75, and 25% were tested. The effect of the CaO addition on the recovery of Ni/Mo/V as well as their content in the slag is shown in Figure 9.

The test results showed that as the CaO content gradually increases from 6.25 to 25.0%, the recovery of Ni, Mo, and V gradually increases. This is mainly because an increase in the CaO content reduces the viscosity and surface tension of the slag. When the CaO content is 25%, the recovery of Ni, Mo, and V is 79.3, 84.9, and 20.7%, respectively. However, compared with the results with no CaO addition, the recovery of all three metals is reduced. It can also be seen that the content of Ni, Mo, and V in the slag rapidly increases after the addition of 6.25% CaO, followed by a decrease with a further increase in the CaO content. When the CaO content was 6.25%, the Fe content in the slag was 23.1%, which is higher than 21.4% Fe for no CaO addition. This may be because the addition of CaO causes changes in the slag composition and the melting point of the slag system, thereby resulting in changes in the degree of reduction and sulfurization of metals,

Table 7. Chemical Composition of the Slag and Matte

element	MgO	Al_2O_3	SiO_2	Fe	S	Ni	Mo	V	Pt (g/t)	Pd (g/t)	Rh (g/t)
slag (wt %)	0.30	21.44	42.18	21.53	0.42	0.17	0.10	0.80	0.03	1.03	0.05
matte (wt %)				61.35	8.89	12.48	9.53	1.90	19.45	181.89	13.97

https://doi.org/10.1021/acsomega.3c05772
ACS Omega 2023, 8, 40713−40728

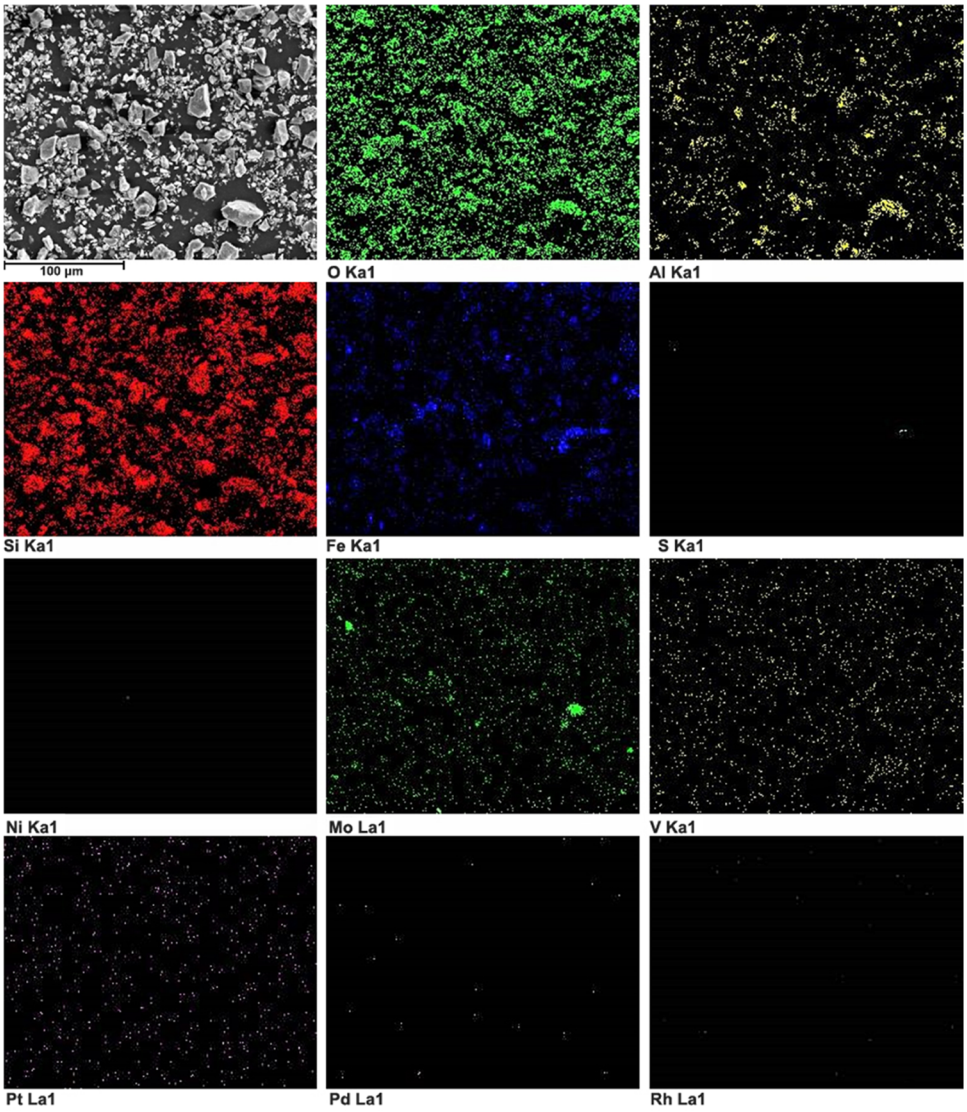

Figure 11. Elemental mapping of smelting slag.

such as Fe and Ni. With a further increase in the CaO content, the Fe content in the slag decreases at a faster rate compared with the Ni, Mo, and V contents. This suggests that an increase in CaO prioritizes the reaction of Fe into the matte phase, thereby consuming more reducing agents and hindering the reduction and sulfurization of the targeting metals. The Ca content in the slag continuously increases with CaO addition from 0.14 to 6.89% for a CaO content of 25%. The smelting slag is an Al_2O_3-FeO-SiO_2-CaO quaternary slag. Based on the above information, no CaO is added to the system for test validation. Since no CaO was needed as an additive, the PGMs were not tested; meanwhile, with the increase of CaO, the Fe content in the slag decreases more significantly compared to Ni, Mo, and V content, indicating that the increase of CaO prioritizes the reaction of Fe into the matte phase, thereby consuming more reducing agents and hindering the reduction and sulfurization of the target valuable metal.

3.3.6. Test Validation. Based on the tests performed, the selected operating conditions are smelting temperature of 1450 °C; smelting time of 2 h, coke addition of 16%; pyrite addition of 25%; and no CaO added. Three tests were performed under these conditions. The results are given in Table 6.

The average recoveries of Ni and Mo are 91.1 and 92.9%, respectively. However, the recovery of V is much lower, i.e., 25.1%. The recoveries of PGMs average 99.0, 96.2, and 97.4% for Pt, Pd, and Rh, respectively. The main elemental compositions of the slag and matte are shown in Table 7

The main components of the slag are Al_2O_3, SiO_2, and FeO, with an approximate ratio of 23:46:31 for Al_2O_3/SiO_2/FeO, located near the 1300 °C melting point of the Al_2O_3-FeO-SiO_2 ternary slag system.

The phases in the slag were also identified by XRD and are shown in Figure 10. The main mineral phases of the slag are cristobalite, spinel, mullite, and olivine. Spinel is the main constituent, while cristobalite is a minor phase, indicating that Al, Si, and Fe are mainly bound together in the form of chemical compounds, while Fe can also exist in spinel and olivine through isomorphic substitution.

Elemental mapping of the smelting slag was also performed using SEM and is shown in Figure 11. It can be seen that O, Al, and Si form aluminosilicate compounds. Fe is clustered and embedded in the compounds, and occasionally, it replaces Al and combines with O and Si. Ni and S are less distributed in the slag. Mo is evenly distributed. V and Pt are uniformly

https://doi.org/10.1021/acsomega.3c05772
ACS Omega 2023, 8, 40713−40728

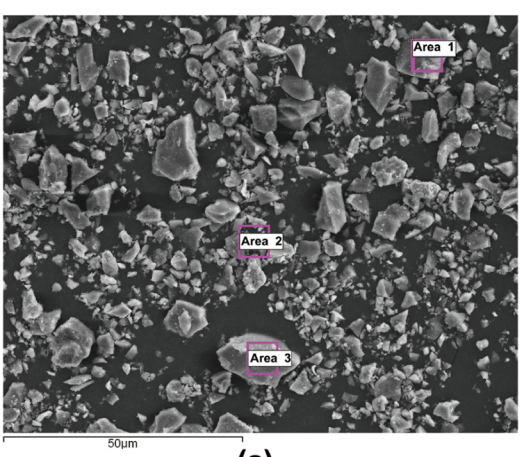

(a)

Element composition and content analysis

Element	Area 1	Area 2	Area 3
O	53.96	51.99	46.90
Fe	10.25	16.97	7.78
Al	14.57	10.09	23.18
Si	18.19	16.63	13.23
S	/	/	/
Ni	/	0.40	/
Mo	/	/	/
V	0.94	1.50	6.19
Pt	2.09	2.41	2.72
Pd	/	/	/
Rh	/	/	/

(b)

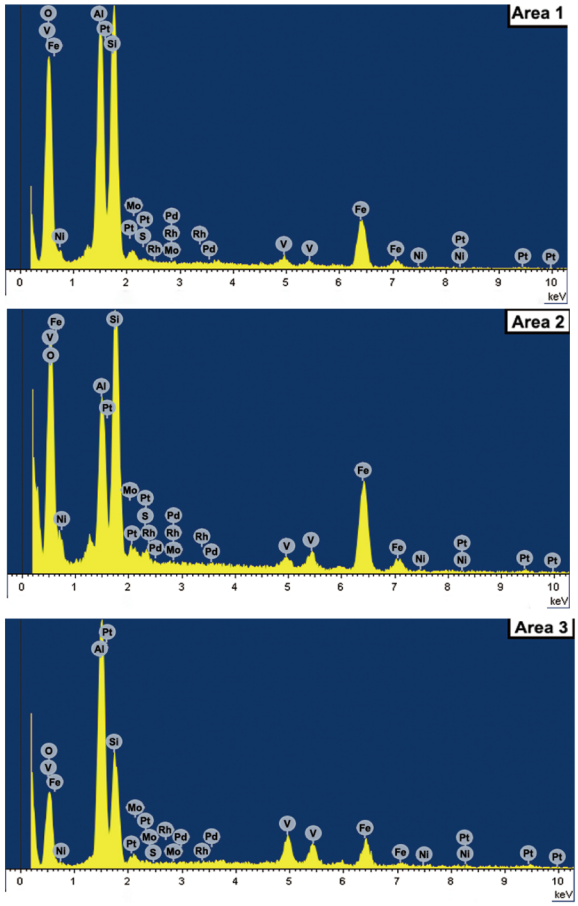

(c)

Figure 12. SEM analyses and EDS results for smelting slag: (a) SEM image of the selected area, (b) element composition and content analysis through EDS, and (c) corresponding spectrograms.

Table 8. Chemical Composition of Garnierite

element	Al_2O_3	SiO_2	CaO	MgO	Fe	Ni	Co	Cr
content (wt %)	2.65	38.33	0.53	20.21	15.63	1.58	0.04	0.74

embedded in the slag. The amounts of Pd and Rh are relatively small and dispersed.

SEM analyses and EDS results for the smelting slag are listed in Figure 12. O, Al, Fe, and Si are the main constituent elements of the slag, while V and Pt are embedded in olivine. This would affect their recovery efficiency. In some locations, V partially replaces Fe. Ni and Mo are rarely embedded in ferro- or aluminosilicate, and cannot be detected by EDS. Ni, Mo, and Fe form compounds without binding to Al.

As concluded from the above, three stages are involved during the formation of the matte: (1) Under high temperatures, the formed liquid phase (Fe-Ni-Mo-V-PGMs-S) fills the pores of the sample. As the liquid phase flows, the particles (Fe-Mo, Fe-Ni, Fe/Al/Ni/Mo-PGMs, and V-S/O) slide, rotate, and rearrange, leading to rapid densification to the body. The liquid phase simultaneously infiltrates and dissolves along the grain boundaries within the particles, washing individual particles into smaller particles; however, V, may be wrapped by the ferro- or aluminosilicate that cannot be dissolved into matte. (2) The grain boundary at the neck of the large particle sweeps toward the direction of small particles, the edges and corners of large particles, microconvex, and fine particles are dissolved in the liquid phase, and the liquid film at the grain boundary migrates. When the concentration of the solid phase in the liquid exceeds the saturation concentration, it reprecipitates on the surface of large particles. (3) With further growth of the neck of particles, the grain grows and the pores coarsen at the same time. It should be noted that the vanadium composition in three different areas varies; this is mainly due to the fact that the analyzed sample is a smelting slag powder with a low vanadium content; it is easy to obtain uneven distribution or segregation in areas with different shapes during the dotting process.

After the reaction temperature exceeds 1000 °C, controlled by the Boudouard reaction, the reduction atmosphere in the furnace is mainly dominated by CO, and according to the $\Delta G-T$ diagrams of eqs 13−23, it can be seen that with FeS_2 in the CO atmosphere, no matter whether to produce FeO or FeS, the ΔG of the oxides of V is obviously higher than that of other metals, which indicates that the V reaction is more difficult to be carried out under the same conditions, and this is also consistent with the fact that the vanadium recovery is lower. According to the ΔG−T diagrams of eqs 26−31, the ΔG of eq 28 is always greater than 0 with increasing

https://doi.org/10.1021/acsomega.3c05772
ACS Omega 2023, 8, 40713−40728

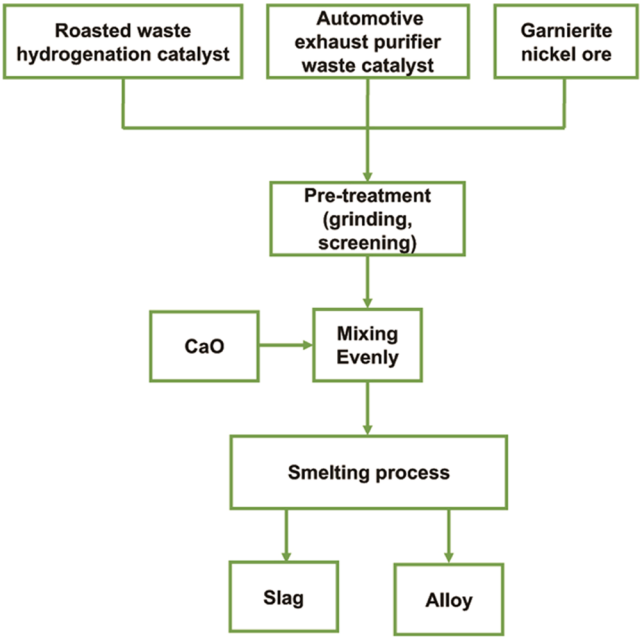

Figure 13. Schematic of the smelting process.

Table 9. Recovery of Valuable Metals Using Garnierite

no.	Ni (%)	Mo (%)	V (%)	Pt (%)	Pd (%)	Rh (%)
1	96.6	96.2	88.3	89.7	98.2	96.6
2	96.8	97.0	90.9	90.2	97.7	92.9
3	97.0	96.8	89.9	90.7	98.1	95.0
average	96.8	96.7	89.7	90.2	98.0	94.9

temperature, while the thermodynamic ΔG of eq 31 is also higher than that of eqs 29 and 30 at the same temperature, and it is only possible to react above 1000 °C, indicating that the vanadium oxides are also more difficult to react directly with iron sulfides in an interactive manner, whereas the reactions of Ni, Mo, and Fe sulfides are easier to carry out under the same conditions.

3.4. Smelting without Sulfurization. Since the laterite nickel ore contains a very high Fe content, the resulting Al_2O_3-FeO-SiO_2 ternary slag system has resulted in a very low V recovery. Thus, another type of nickel ore (garnierite) containing much less Fe and higher MgO was tested, which could help form the Al_2O_3-MgO-SiO_2 ternary slag system. The main composition of garnierite is given in Table 8.

A schematic of the smelting process is shown in Figure 13.

As compared with Figure 1, it can be seen that no pyrite and coke was added to the catalysts; through smelting tests, the operating conditions could be listed as follows: smelting temperature of 1525 °C, smelting time of 2 h, garnierite to catalyst ratio of 1.5, and CaO addition of 7.5%. It should be noted that this type of slag has a high content of silicon and magnesium, resulting in a higher viscosity and density for the slag. The addition of CaO can reduce the viscosity and density of the slag, optimize the fluidity of the slag, and promote ferro- or nickel silicate dissociates into simple oxides. Thus, it was added to this process. Three parallel tests were performed, and the results are shown in Table 9.

The main elemental compositions of the slag and matte are shown in Table 10

It can be seen that Al_2O_3, MgO, and SiO_2 are the main components of the slag, with an approximate conversion ratio of Al_2O_3/MgO/SiO_2 of 25:29:46, which means that it is located in the lower melting point region of the ternary Al_2O_3-MgO-SiO_2 slag system. The Ni, Mo, and V content in the slag is less than 0.1%. The difference between the V recovery in Sections 3.4 and 3.5 could be explained that initially, V has a high melting temperature (1890 °C) due to a smaller atomic radius (1.92 Å), bringing a stronger electrostatic interaction between metal cations and free electrons, thus bringing a high temperature to break its stronger metallic bonding. For Mo and Ni, their valence electrons are not easy to lose, and they have weak affinity with oxygen and sulfur, they have affinity to iron, and they are easy to be concentrated into the Fe-Ni core, as shown in both Sections 3.4 and 3.5 that the matte contains a high concentration of iron; different from Mo, Ni, and PGMs, V atom has an out layer with eight electrons, which could form a stable ionic bond compound with oxygen and easy to melt in silicate melt, whereas satisfying conditions in Section 3.4 are not guaranteed due to much higher concentration of sulfur; in addition, the melting temperature selected in Section 3.5 is 1525 °C, higher than the temperature selected in Section 3.4 (1450 °C); this is due to the fact that the Al_2O_3-MgO-SiO_2 slag system has a higher melting point liquidus than the Al_2O_3-FeO-SiO_2 slag, thus bringing a higher energy as well as lower viscosity for V to be captured by matte.

4. CONCLUSIONS

Combined reduction−sulfurization smelting treatment of WHCs, spent automotive catalysts, and laterite nickel ore has been explored. At a melting temperature of 1450 °C, melting time of 2 h, and mass ratio of coke, pyrite, and CaO to waste catalysts of 16, 25, and 0%, recovery of the valuable metals, including nickel, molybdenum, and PGMs (Pt, Pd, Rh), reached 91.1, 92.9, and 96%, respectively, although vanadium recovery was only 25.1%. In general, with an increase in melting temperature, melting time, and mass ratio of coke, the recovery rates of Ni, Mo, V, and PGMs gradually increase. However, the impact of the mass ratio of pyrite is different. However, an increase in Ni, Mo, V, and PGMs recovery can be seen in the initialing, and the recovery then decreases as the mass ratio of pyrite further increases. This is due to the increased pyrite content that results in a very high FeO content in the slag. To explore the possibility of increasing V recovery, the Al_2O_3-FeO-SiO_2 slag system was changed into an Al_2O_3-MgO-SiO_2 slag system by replacing the laterite nickel ore with a low-Fe and high-Mg garnierite without any pyrite or coke addition. The results showed that at a melting temperature of 1525 °C, smelting time of 2 h, garnierite to catalysts ratio of 1.5, and CaO addition of 7.5%, Ni, Mo, V, and PGMs average recovery reached 96.82, 96.66, 89.69, and 94.3%, respectively.

Table 10. Chemical Composition of the Slag and Matte

element	MgO	Al_2O_3	SiO_2	CaO	Fe	Ni	Mo	V	Pt (g/t)	Pd (g/t)	Rh (g/t)
slag (wt %)	21.47	25.06	40.32	4.91	0.86	0.07	0.04	0.09	0.40	0.91	<0.1
matte (wt %)			4.96	1.53	67.59	11.90	5.82	4.35	18.54	193.17	14.50

https://doi.org/10.1021/acsomega.3c05772
ACS Omega 2023, 8, 40713−40728

The major difference in V recovery between reduction−sulfurization smelting and reduction smelting process lies in V's specific valence and bonding characteristics and difference in melting temperatures resulting from different slag types.

AUTHOR INFORMATION

Corresponding Author

Hao Ma − *BGRIMM Technology Group, Beijing 100070, China*; orcid.org/0000-0001-7253-734X; Email: haoma@bgrimm.com

Authors

Zihao Wang − *BGRIMM Technology Group, Beijing 100070, China*

Haibei Wang − *BGRIMM Technology Group, Beijing 100070, China*

XiaoWu Jie − *BGRIMM Technology Group, Beijing 100070, China*

Xu Zhao − *BGRIMM Technology Group, Beijing 100070, China*

Kristian E. Waters − *Department of Mining and Materials Engineering, McGill University, Montreal, Quebec, Canada H3A 0C5*

Derek O. Northwood − *Department of Mechanical, Automotive and Materials Engineering, University of Windsor, Windsor, Ontario, Canada N9B3P4*

Senlin Cui − *School of Civil Aviation, Northwestern Polytechnical University, Xi'an, Shaanxi 710072, China*

Complete contact information is available at: https://pubs.acs.org/10.1021/acsomega.3c05772

Notes

The authors declare no competing financial interest.

ACKNOWLEDGMENTS

The support from the National Key Research and Development Program (2022YFC3902005) from the Ministry of Science and Technology of China is acknowledged. The support from China Minmetals Corporation (2021ZXD01) is also acknowledged.

REFERENCES

(1) Xiu, S.; Shahbazi, A. Bio-oil production and upgrading research: A review. *Renewable Sustainable Energy Rev.* **2012**, *16* (7), 4406−4414.

(2) Le, M. N.; Lee, M. S. A review on hydrometallurgical processes for the recovery of valuable metals from spent catalysts and life cycle analysis perspective. *Miner. Process. Extr. Metall. Rev.* **2021**, *42* (5), 335−354.

(3) Dias, J. A.; Assaf, J. M. Autothermal reforming of methane over Ni/γ-Al_2O_3 catalysts: the enhancement effect of small quantities of noble metals. *J. Power Sources* **2004**, *130* (1−2), 106−110.

(4) Corro, G.; Cruz-Mérida, J.; Montalvo, D.; Pal, U. Performance of Pt/Cr_2O_3, Pt/ZrO_2, and, Pt/γ-Al_2O_3 catalysts in total oxidation of methane: effect of metal−support interaction. *Ind. Eng. Chem. Res.* **2021**, *60* (51), 18841−18852.

(5) Doi, K.; Wu, Y. Y.; Takeda, R.; Matsunami, A.; Arai, N.; Tagawa, T.; Goto, S. Catalytic decomposition of N_2O in medical operating rooms over Rh/Al_2O_3, Pd/Al_2O_3, and Pt/Al_2O_3. *Appl. Catal., B* **2001**, *35* (1), 43−51.

(6) Cempel, M.; Nikel, G. J. P. J. S. Nickel: A review of its sources and environmental toxicology. *Pol. J. Environ. Stud.* **2006**, *15* (3), 375−382.

(7) Sun, W.; Li, X.; Liu, R.; Zhai, Q.; Li, J. Recovery of valuable metals from nickel smelting slag based on reduction and sulfurization modification. *Minerals* **2021**, *11* (9), 1022.

(8) Su, K.; Wang, F.; Parianos, J.; Cui, Z.; Zhao, B.; Ma, X. Alternative resources for producing nickel matte-laterite ores and polymetallic nodules. *Miner. Process. Extr. Metall. Rev.* **2022**, *43* (5), 584−597.

(9) Wang, X.; Zhu, D.; Guo, Z.; Pan, J.; Lv, T.; Yang, C.; Li, S. Efficient utilization of limonite nickel laterite to prepare ferronickel by the selective reduction smelting process. *Sustainability* **2023**, *15* (9), 7147.

(10) Anameric, B.; Kawatra, S. K. Direct iron smelting reduction processes. *Miner. Process. Extr. Metall. Rev.* **2008**, *30* (1), 1−51.

(11) Wang, Y.; Zhu, R.; Chen, Q.; Wei, G.; Hu, S.; Guo, Y. Recovery of Fe, Ni, Co, and Cu from nickel converter slag through oxidation and reduction. *ISIJ Int.* **2018**, *58* (12), 2191−2199.

(12) Li, Y.; Chen, Y.; Tang, C.; Yang, S.; He, J.; Tang, M. Co-treatment of waste smelting slags and gypsum wastes via reductive-sulfurizing smelting for valuable metals recovery. *J. Hazard. Mater.* **2017**, *322*, 402−412.

(13) Guo, Y.; Jing, J.; Chen, F.; Wang, S.; Yang, L. Selective separation of tin from tin-bearing middling via sulfur roasting. *Environ. Technol. Innovation* **2022**, *27*, No. 102545.

(14) Cao, S.; Chang, L.; Bi, X.; Luo, S.; Liu, J. The extraction of silica from nickel laterite ore by alkaline hydrothermal process. *Min., Metall., Explor.* **2022**, *39* (3), 1245−1253.

(15) Whitworth, A. J.; Vaughan, J.; Southam, G.; van der Ent, A.; Nkrumah, P. N.; Ma, X.; Parbhakar-Fox, A. Review on metal extraction technologies suitable for critical metal recovery from mining and processing wastes. *Miner. Eng.* **2022**, *182*, No. 107537, DOI: 10.1016/j.mineng.2022.107537.

(16) Kartini, E.; Fakhrudin, M.; Astuti, W.; Sumardi, S.; Mubarok, M. Z. In *The Study of (Ni, Mn, Co) SO4 as Raw Material for NMC Precursor in Lithium Ion Battery*, AIP Conference Proceedings, AIP Publishing LLC, 2022; Vol. 2708, No. 1, p. 070001.

(17) Razavian, M.; Fatemi, S.; Najafabadi, A. T. Extraction of highly pure nickel hydroxide from spent NiO/Al2O3 catalyst: statistical study on leaching by sulfuric acid lixiviant and selective precipitation. *J. Environ. Chem. Eng.* **2020**, *8* (2), No. 103660.

(18) Wang, M.; Wei, C.; Fan, G.; Li, M.; Deng, Z.; Wang, S. Selective extraction of Mo from a Ni−Mo ore using pressure alkaline leaching. *Hydrometallurgy* **2015**, *153*, 6−11.

(19) Laungsakulthai, K.; Chandakhiaw, T.; Wongnaree, N.; Thampiriyanon, J.; Kritsarikun, W.; Khumkoa, S. Smelting Reduction of Spent Catalyst Containing Nickel: A Preliminary Study. In *Materials Science Forum*, Trans Tech Publications Ltd.: 2020; Vol. *1009*, pp. 162−167.

(20) Pak, J. J.; Kim, D. H.; Paek, M. K.; Kim, Y. D. Ferroalloy Production from Spent Petroleum Catalysts by Reductive Smelting and Selective Oxidation Processes. In *REWAS 2019: Manufacturing the Circular Materials Economy*; Springer International Publishing, 2019; pp 167−175.

(21) Ilhan, S. Extraction of molybdenum, nickel and aluminium from spent Ni−Mo hydrodesulphurization (HDS) catalyst in oxalic acid solutions. *Can. Metall. Q.* **2020**, *59* (1), 26−35.

(22) Zhang, D.; Liu, Y.; Hu, Q.; Ke, X.; Yuan, S.; Liu, S.; Ji, X.; Hu, J. Sustainable recovery of nickel, molybdenum, and vanadium from spent hydroprocessing catalysts by an integrated selective route. *J. Cleaner Prod.* **2020**, *252*, No. 119763.

(23) Ko, J. H.; Wang, Q.; Yuan, T.; Wu, H.; Xu, Q. Geotextile clogging at different stages of municipal solid waste landfills co-disposed with bottom ash. *Sci. Total Environ.* **2019**, *687*, 161−167.

(24) Melendi, S.; Diez, M. A.; Alvarez, R.; Barriocanal, C. Plastic wastes, lube oils and carbochemical products as secondary feedstocks for blast-furnace coke production. *Fuel Process. Technol.* **2011**, *92* (3), 471−478.

(25) Guo, Z.; Pan, J.; Zhu, D.; Zhang, F. Green and efficient utilization of waste ferric-oxide desulfurizer to clean waste copper slag by the smelting reduction-sulfurizing process. *J. Cleaner Prod.* **2018**, *199*, 891−899.

(26) Fornalczyk, A. Industrial catalysts as a source of valuable metals. *J. Achiev. Mater. Manuf. Eng.* **2012**, *55* (2), 864−868.

(27) Crundwell, F.; Moats, M.; Ramachandran, V.; Robinson, T.; Davenport, W. G. *Extractive Metallurgy of Nickel, Cobalt and Platinum Group Metals*; Elsevier, 2011.
(28) Zheng, C.; Jiang, K.; Cao, Z.; Wang, H.; Liu, S.; Waters, K. E.; Ma, H. Pressure leaching behaviors of copper-cobalt sulfide concentrate from Congo. *Sep. Purif. Technol.* **2023**, *309*, No. 123010.
(29) Nadirov, R. K.; Syzdykova, L. I.; Zhussupova, A. K.; Usserbaev, M. T. Recovery of value metals from copper smelter slag by ammonium chloride treatment. *Int. J. Miner. Process.* **2013**, *124*, 145−149.
(30) Liu, Y.; Sotelo-Boyás, R.; Murata, K.; Minowa, T.; Sakanishi, K. Production of bio-hydrogenated diesel by hydrotreatment of high-acid-value waste cooking oil over ruthenium catalyst supported on Al-polyoxocation-pillared montmorillonite. *Catalysts* **2012**, *2* (1), 171−190.
(31) Marafi, M.; Stanislaus, A. Spent catalyst waste management: A review: Part I—Developments in hydroprocessing catalyst waste reduction and use. *Resour., Conserv. Recycl.* **2008**, *52* (6), 859−873.
(32) Yang, Q. Z.; Qi, G. J.; Low, H. C.; Song, B. Sustainable recovery of nickel from spent hydrogenation catalyst: economics, emissions and wastes assessment. *J. Cleaner Prod.* **2011**, *19* (4), 365−375.
(33) Zeng, L.; Cheng, C. Y. A literature review of the recovery of molybdenum and vanadium from spent hydrodesulphurisation catalysts: Part I: Metallurgical processes. *Hydrometallurgy* **2009**, *98* (1−2), 1−9.
(34) Wang, W.; Wang, S.; Ma, X.; Gong, J. Recent advances in catalytic hydrogenation of carbon dioxide. *Chem. Soc. Rev.* **2011**, *40* (7), 3703−3727.
(35) Guo, Z.; Wang, X. Atomic layer deposition of the metal pyrites FeS_2, CoS_2, and NiS_2. *Angew. Chem., Int. Ed.* **2018**, *57* (20), 5898−5902.
(36) Font, J. M.; Hino, M.; Itagaki, K. Minor elements distribution between iron-silicate base slag and Ni3S2−FeS matte under high partial pressures of SO_2. *Mater. Trans., JIM* **1998**, *39* (8), 834−840.
(37) Marakushev, A. A.; Bezmen, N. I. Chemical affinity of metals for oxygen and sulfur. *Int. Geol. Rev.* **1971**, *13* (12), 1781−1794.
(38) Lee, M.; Oh, H. S.; Cho, M. K.; Ahn, J. P.; Hwang, Y. J.; Min, B. K. Activation of a Ni electrocatalyst through spontaneous transformation of nickel sulfide to nickel hydroxide in an oxygen evolution reaction. *Appl. Catal., B* **2018**, *233*, 130−135.
(39) Zhang, J.; Yang, C.; Chen, Y.; Wang, C. Efficient phase transformation of γ-Al_2O_3 to α-Al_2O_3 in spent hydrodesulphurization catalyst by microwave roasting method. *Ind. Eng. Chem. Res.* **2019**, *58* (4), 1495−1501.
(40) Düvel, A.; Romanova, E.; Sharifi, M.; Freude, D.; Wark, M.; Heitjans, P.; Wilkening, M. Mechanically induced phase transformation of γ-Al_2O_3 into α-Al_2O_3. Access to structurally disordered γ-Al_2O_3 with a controllable amount of pentacoordinated Al sites. *J. Phys. Chem. C* **2011**, *115* (46), 22770−22780.

https://doi.org/10.1021/acsomega.3c05772
ACS Omega 2023, 8, 40713−40728